Simultaneous excitation and ionization of He-like uranium ions in relativistic collisions with gaseous targets

T. Ludziejewski*
Gesellschaft für Schwerionenforschung, 64220 Darmstadt, Germany
and Andrzej Sołtan Institute for Nuclear Studies, 05-400 Świerk, Poland

Th. Stöhlker
Institut für Kernphysik, University of Frankfurt, August-Euler-Straße 6, D-60486 Frankfurt, Germany
and Gesellschaft für Schwerionenforschung, 64220 Darmstadt, Germany

D. C. Ionescu
Lawrence Berkeley National Laboratory, 1 Cyclotron Road, Berkeley, California 94720

P. Rymuza
Andrzej Sołtan Institute for Nuclear Studies, 05-400 Świerk, Poland

H. Beyer, F. Bosch, C.Kozhuharov, A. Krämer, D. Liesen, and P. H. Mokler
Gesellschaft für Schwerionenforschung, 64220 Darmstadt, Germany

Z. Stachura
Institute of Nuclear Physics, 31-342 Cracow, Poland

P. Świat and A. Warczak
Institute of Physics, Jagiellonian University, 30-059 Cracow, Poland

R. W. Dunford
Argonne National Laboratory, Argonne, Illinois 60439
(Received 21 June 1999; published 7 April 2000)

The process of simultaneous excitation and ionization is investigated for He-like uranium (U^{90+}) ions colliding with Ar, Kr, and Xe targets at an incident energy of 223.2 MeV/u. The two-electron transitions, where one of the ground-state electrons is promoted into the continuum and the other into the *L*-subshell states of the projectile, are identified by the coincident observation of U Lyman-series radiation and U^{91+} ions. The experimental cross sections are compared to relativistic calculations based on the independent particle approximation and first-order perturbation theory. It is shown, that simultaneous excitation-ionization occurs preferably at small impact parameters, for which the excitation process is dominated by the monopole part of the interaction potential and the perturbation potential is largest. Good agreement is found between experimental data and calculations for the Ar target. For heavier targets the experimental results are generally smaller than predicted pointing to the invalidity of the first-order perturbation theory in this energy–target atomic number domain.

PACS number(s): 34.50.Fa

I. INTRODUCTION

In recent years, a substantial amount of experimental data has been collected for a variety of fundamental processes occurring in relativistic or ultra-relativistic collisions of high-Z ions with atoms (for a review see, e.g., Refs. [1] and [2]). These studies encompass such processes as radiative (REC) and nonradiative (NRC) electron capture [3–6], electron capture from pair production [7–9], as well as target and projectile ionization [8–14]. Progress in the experimental field has been accompanied by a more refined theoretical description incorporating a fully relativistic treatment, which quite often goes beyond a perturbative approach [15–22].

In contrast to charge exchange processes, there are almost no experimental data available for electron excitation of high-Z ions in relativistic ion-atom collisions. Recently, the first study of this type has been reported for the case of *K*-shell electron excitation of H- and He-like Bi (Z=83) ions [23,24]. It has been shown that even at moderately relativistic energies ($\beta = v_{proj.}/c \simeq 0.46$ where $v_{proj.}$ is the projectile velocity, and c is the speed of light), ground state excitation has to be described in terms of the coherent sum of magnetic and electric amplitudes of the complete interaction potential. In that case, the inclusion of magnetic term leads to destructive interference resulting in a reduction of the total excitation cross sections, as compared to the quasi-relativistic approach, in which the electric and magnetic parts of the

*Electronic address: T.Ludziejewski@gsi.de

interaction potential are added incoherently.

Previous studies of the dynamics of relativistic ion-atom collisions focussed on single-electron processes. In this paper we report on an investigation of the simultaneous (i.e., occurring in a single-ion-atom collision) excitation and ionization of He-like uranium at relativistic collision velocities ($\beta = 0.59$). Many-electron processes have been studied extensively, both experimentally and theoretically, mainly for nonrelativistic systems due to the fundamental question of the role of electron-correlation in the dynamics of the ion-atom collisions (for a review see, e.g., Ref. [25], and references therein). Also the process of simultaneous excitation and ionization has been addressed in that context [26–28]. Our study provides a complement to the experimental data for the domain of strong Coulomb fields and for energies, where relativistic effects play an important role.

In the experiment 223.2 MeV/u U^{90+} ions colliding with gaseous Ar, Kr, and Xe targets were used. The identification of excitation-ionization events are greatly facilitated in the case of He-like projectile, since electron capture cannot lead to ground state x-ray emission due to the initially occupied K-shell, and no x-ray emission due to the deexcitation of spectator electrons is possible. Excitation-ionization cross sections could be, in this case, determined directly from the uranium Ly-α-series radiation measured in coincidence with projectiles having lost one electron (U^{91+} ions). The experimental data are compared to the relativistic calculations based on the perturbation theory and the independent particle model (IPM). Two issues are addressed in the discussion. First, we examine the relevance of a fully relativistic perturbative description of the projectile excitation accompanied by ionization. Second, we investigate the validity of the independent particle model for the description of this process for a highly charged high-Z system. Apart from providing these applicability criteria, our data allow us to establish a scaling law for excitation plus ionization cross sections with the target atomic number.

The paper is organized as follows: in Sec. II the experimental arrangement is discussed, Sec. III gives a brief overview of the theoretical methods used for the description of simultaneous excitation and ionization. The applied method of data analysis is discussed in Sec. IV. In Sec. V we show the experimental cross sections for the simultaneous excitation and ionization of U^{90+} ions and compare them to the theory. We conclude with a summary in Sec. VI.

II. EXPERIMENTAL PROCEDURE

The experiment was carried out at the SIS-ESR (Heavy Ion Synchrotron-Experimental Storage Ring) facility at the Gesselschaft für Schwerionenforschung in Darmstadt. Uranium ions with energies of approximately 223 MeV/u were delivered by the SIS accelerator. After passing through a copper stripper foil, each beam pulse was magnetically analyzed, and a fraction of U^{90+} ions were injected into the ESR storage ring. The stored beam was cooled by the electron cooler device operating at 121.670 kV and 100–150 mA. The beam stacking was continued until approximately 10^8 uranium ions were accumulated in the ring. Subsequently, a supersonic gas-jet target was switched on. Argon, krypton, and xenon targets with areal densities between 10^{11} and 10^{12} particles/cm^2 were used in the measurements. The final beam energy equal to 223.2 MeV/u was defined by the voltage of the electron cooler. The cooler, operating continuously during the accumulation and measurement phase, compensated for small beam energy losses due to the interaction with target atoms and rest gas, and provided excellent quality beams with typical diameter $\Phi = 2-3$ mm, a momentum spread $\delta p/p \leqslant 10^{-4}$, and the corresponding transverse emittance of the order of 0.1π mm mrad.

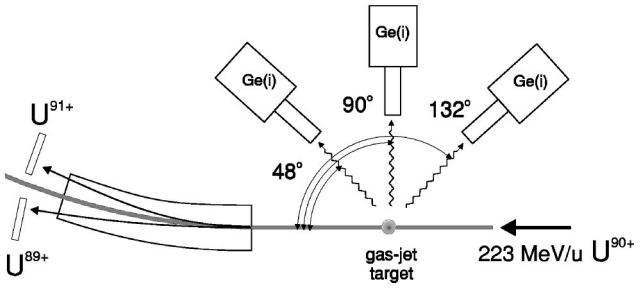

FIG. 1. Simplified diagram of the experimental arrangement at the internal gas-jet target of the ESR.

A schematic arrangement of the detector setup at the target area of the ESR storage ring is shown in Fig. 1. X-rays emitted from the beam-target interaction zone were measured by three thick planar Ge(i) detectors placed at observation angles of 48°, 90°, and 132° with respect to the beam direction. The detectors placed at 48° and 132° were separated from the ultra-high-vacuum system of the ESR storage ring by 100 μm-thick beryllium windows, while a 50 μm-thick stainless steel window was used at 90°. For x-ray energies of interest, the absorption in the windows was negligible. In order to keep the Doppler broadening of the lines small enough to resolve Lyα_1 and Lyα_2 radiation of the projectile, the solid angle subtended by the detectors had to be confined. For this purpose, a slotted copper and lead assembly with 5 mm wide opening was mounted directly in front of the detectors placed at 48° and 90°.

After passing through the target, the beam was charge state separated at the first magnetic bend of the ring. Fractions of U^{91+} and U^{89+} ions were directed into the particle detectors located in the inner and outer part of the ring. The detectors used (NE110 plastic scintillator counters) registered down-charged (Li-like), and up-charged (H-like) uranium ions with efficiency very close to 100%.

Signals were processed employing standard data taking techniques based on CAMAC and NIM electronics. The data collection was carried out in successive accumulation-measurement cycles until a required statistical significance (better than 15% for two-electron processes) was achieved. Two data acquisition modes were maintained; coincidence mode, and single mode (no coincidence with particle counters). The latter allows for the detailed study of the single-excitation process for He-like uranium. This will be done in a forthcoming paper.

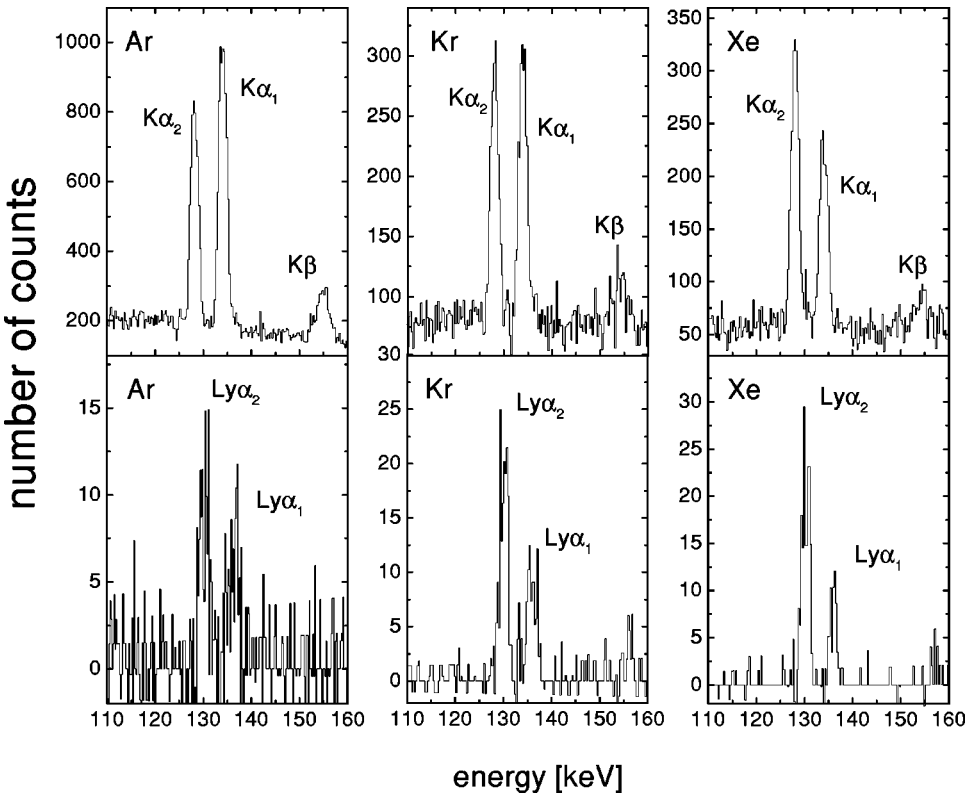

FIG. 2. Sample x-ray spectra recorded at 48° for initially He-like uranium ions colliding with Ar, Kr, and Xe gas target atoms. The upper plots represent single spectra (projectile excitation). The lower plots represent spectra recorded with simultaneous condition of ionization of the projectile (projectile excitation plus ionization). Both single and coincidence spectra were corrected for efficiency of the Ge(i) detector. The coincidence spectra were additionally corrected for random events.

Projectile $K\alpha$, Ly-α radiation

For He-like systems where the $nlj \rightarrow 1s$ transitions following electron capture processes are forbidden by the Pauli exclusion principle, the observation of ground-state x-ray transitions constitutes the direct signature of a ground-state excitation. Likewise, the simultaneous ionization and excitation into nlj states can be identified through the observation of ground state x-ray emission in coincidence with up-charged (H-like) projectiles. It is important to note here, that in the standard experiments with solid targets, a measurement of two-electron processes is not feasible due to the prohibitively high probabilities of excitation and ionization occurring in two successive collisions. In contrast, for gas targets with typical areal densities of 10^{12} particles/cm^2 the probability for such a two-step excitation-ionization process is negligible. Moreover, due to the large fine-structure splitting for H-like U the transitions from states with total angular momentum $j=1/2$ are well separated from those with $j=3/2$. Therefore, the cross sections for simultaneous ionization and excitation into the different total angular momentum states of the $n=2$ shell can be directly determined from the observed yields of Lyα_1 and Lyα_2 radiation of the projectile.

In Fig. 2, x-ray spectra recorded for 223.2 MeV/u initially He-like U^{90+} ions impinging upon Ar, Kr, and Xe gas targets are plotted. To illustrate the differences between single excitation and simultaneous excitation plus ionization both excitation modes are shown. The upper plots show data taken at an observation angle equal to 48° without coincidence conditions. The prominent, well resolved $K\alpha_2$ and $K\alpha_1$ emission lines due to ground-state electron excitation into the L-shell projectile states can be seen. It is interesting to note that for the case of single excitation, the $K\alpha_2/K\alpha_1$ intensity ratio changes markedly with target atomic number.

The lower part of Fig. 2 shows the corresponding spectra recorded in coincidence with projectile ionization. Since in that case the x-ray transitions occur in H-like ions, positions of $2j \rightarrow 1s$ $(j=1/2,3/2)$ lines appear markedly shifted in energy with respect to single excitation. Moreover, a significant change in the ratio of relative intensities of Lyα_2:Lyα_1 lines (ionization plus excitation) with respect to $K\alpha_2$:$K\alpha_1$ (excitation) can be seen. To understand this striking difference one has to consider different decay modes of s-levels in H- and He-like heavy ions. For He-like systems the population of 2^1S_0 state does not lead to the emission of $K\alpha$ photons. Instead, this level decays by two-photon (2E1) emission [35]. Therefore, only excitation into 2^3P_1 (and a small admixture of spin-flip populated 2^3S_1, 2^3P_0 states) leads to the production of $K\alpha_2$ x-rays. In contrast, for high-Z H-like ions, the $2s_{1/2}$ state decays by a prompt (M1) transition feeding the Lyα_2 line. Furthermore, the change of relative $K\alpha_2$:$K\alpha_1$ and Lyα_2:Lyα_1 ratios is enhanced by the impact parameter characteristics of the two-electron and the single electron processes. This will be discussed in the following section.

III. THEORETICAL DESCRIPTION OF EXCITATION PLUS IONIZATION PROCESSES

Our theoretical description of simultaneous excitation and ionization of the He-like system relies on two assumptions. First, the process is described within the framework of an independent particle approximation, which postulates that the change of state of one electron does not affect the other one. In other words, we assume that the process of simulta-

neous excitation plus ionization is not correlated. Further, describing single-electron processes, we assume that the inter-nuclear motion can be treated classically, that is, that the collision can be characterized by an impact parameter b. The motivation for this approach is that the generally many-body problem we deal with, can be reduced to a single-electron problem. More specifically, in this approach the probability $p_{nlj}^{\text{ion-exc}}$ for a simultaneous ionization and excitation of the ground-state electrons into the final nlj state of the projectile, can be expressed as an (uncorrelated) product of single-electron probabilities:

$$p_{nlj}^{\text{ion-exc}}(b) \approx 2p^{\text{ion}}(b)p_{nlj}^{\text{exc}}(b). \tag{1}$$

Here, $p^{\text{ion}}(b)$ is the single-electron ionization probability for collision with impact parameter b, $p_{nlj}^{\text{exc}}(b)$ is the single-electron excitation probability into the state characterized by quantum numbers nlj.

Expression (1) assumes that the bound projectile electrons are ejected simultaneously and are subject to the same binding energy. The total cross section for simultaneous excitation and ionization into the nlj state of the projectile is then given by

$$\sigma_{nlj}^{\text{ion-exc}} = \int_0^\infty 2\pi b p_{nlj}^{\text{ion-exc}}(b)db. \tag{2}$$

With the help of Eqs. (1) and (2), the scaling of the cross section for the excitation plus ionization process with target atomic number can be derived. As we use first-order perturbation theory to calculate the single-electron probabilities for excitation and ionization processes, and both scale with Z_T^2 (Z_T is the target atomic number), $\sigma_{nlj}^{\text{ion-exc}}$ should be proportional to Z_T^4. It is worth noting however, that within the first order perturbation theory the probabilities $p^{\text{ion}}(b)$ and $p^{\text{exc}}(b)$ are not mutually exclusive [i.e., $p^{\text{ion}}(b) + \Sigma_{nlj} p_{nlj}^{\text{exc}}(b) + p^{\text{elas}} \neq 1$, where p^{elas} is the probability that the electron does not change the state], and therefore Eq. (1) is in this framework only an approximation.

Since in the present work excitation plus ionization has been investigated for a relatively wide range of target atomic numbers, this scaling can be verified experimentally. In Secs. III A and III B a brief overview of the theoretical approach used to describe the single electron probabilities $p^{\text{ion}}(b)$, and $p^{\text{exc}}(b)$ is given.

A. Ionization probabilities

The description of simultaneous excitation and ionization within the IPA framework requires an impact parameter formulation of individual single-electron processes [see Eqs. (1) and (2)]. For the description of impact parameter dependent ionization we adopted a semi-classical-approximation (SCA) originally developed by Bang and Hansteen [29]. In the SCA, the ionization probability $p^{\text{ion}}(b)$ is determined within first-order perturbation theory assuming that the perturbation potential can be derived according to the classical inter-nuclear trajectory. Calculations were performed with the SCA code of Trautmann and Rösel [30], which exploits relativistic hydrogenic-like wave-functions for the description of the bound state of the projectile electron. A theoretical binding energy of H-like uranium [31], and the continuum electron states with angular momentum $0 \leqslant l \leqslant 4$ were used. Although in the SCA calculations the correct relativistic Dirac bound-state and continuum-state wave-functions are used, this model neglects the magnetic part of the full interaction potential, and assumes nonrelativistic collision kinematics. The latter, is accounted for in our calculations adopting a collision energy for which the projectile velocity matches that given by the relativistic expression.

The magnetic contribution to the total ionization amplitude arises if one considers a relativistic collision where the perturbing spherically-symmetrical Coulombic potential is Lorentz transformed to the reference frame of the ionized atom. This transformation leads to the extension of the potential in the transverse direction and shrinkage in the longitudinal direction, yielding the Liénard-Wiechert potential [2]. The corrections to the cross sections accounting for the magnetic interaction (the so-called transverse and spin-flip contribution) has been calculated by Anholt [32] within the dipole-approximation. Since within this picture, the magnetic part of the interaction amplitude is added incoherently, this correction leads to an increase of the total ionization cross sections with increasing β values. For our moderate β value the magnetic (transverse plus spin flip) part of the ionization cross section accounts only for $\sim 5\%$ of the total ionization cross section. Moreover due to the geometrical properties of the Lorentz transformation of the interaction potential these corrections are most important at large impact parameters [15,33]. It should be noted, that the model proposed by Anholt *et al.* [32], where electric and magnetic contributions are added incoherently, generally yields fairly good agreement with the existing experimental cross section data [12–14], with one interesting exception at ultrarelativistic energies [9].

B. Excitation probabilities

Since the theoretical approach used for the description of the excitation process has been described in detail elsewhere [23], only a brief summary will be given here. For the description of electron excitation a fully relativistic calculations considering a complete (Liénard-Wiechert) interaction potential has been used. In the impact parameter picture, as in the case of ionization, the cross section for excitation is given by

$$\sigma_{fi} = 2\pi \int_0^\infty |A_{\text{fi}}^{\text{e}}|^2 b \, \text{d}b. \tag{3}$$

Within first-order perturbation theory, the transition amplitude in a strictly relativistic formalism has the form [2]

$$A_{fi}^{\text{e}}(b) = \text{i}\frac{\gamma Z_T e^2}{\hbar} \int \text{d}t \text{e}^{i(E_f - E_i)t/\hbar} \int \text{d}^3 r \varphi_f^\dagger(\vec{r}) \times (1 - \beta\alpha_z)\frac{1}{r'}\varphi_i(\vec{r}) \tag{4}$$

Here, E_i, φ_i, and E_f φ_f are the energies and the initial and final eigenstates, respectively, and α_z is the Dirac matrix component in the direction of projectile movement. The space coordinate r' is calculated within the Lorentz gauge assuming that the projectile is moving along the classical trajectory with an impact parameter b characterizing the collision. For the description of initial and final electron states the Coulomb-Dirac wave-functions are used. In the transition matrix element of Eq. (4), the two contributions to the transition amplitude arise from the scalar and the vector parts of the Liénard-Wiechert potential and add up coherently. The importance of the magnetic part of the interaction potential has been recently pointed out for the case of ground-state excitation of H- and He-like bismuth ions in relativistic collisions with low-Z solid targets [23]. It was found that even for moderate β values the electric and magnetic parts of the Liénard-Wiechert interaction interfere leading to a reduction of the absolute magnitude of total cross sections as compared to calculations where only the electric part is considered. This feature of the excitation cross sections, rigorously calculated according to Eq. (4) is distinctly different from that proposed by Anholt *et al.* for ionization [32], where no interference effects are present.

C. Probabilities of simultaneous excitation and ionization in the IPA framework

Figure 3 summarizes the results of calculations described in the preceding sections. Since our theoretical approach is based on first order perturbation theory implying the Z_T^2 scaling law for the probabilities of individual single-electron processes, the reduced values $bp(b)/Z_T^2$ are shown. The curves representing calculated probabilities of individual single-electron processes for 223.2 MeV/u U^{91+} projectiles are depicted in Fig. 3(a). In the case of excitation, only probabilities for the population of the $2s_{1/2}$, $2p_{1/2}$, and $2p_{3/2}$ states summed over the final magnetic sub-states are presented. Also shown, is the probability for K-shell ionization of U^{91+} calculated within the SCA framework neglecting the contribution of the magnetic terms to the ionization probability. We note that the single-excitation mode leads to an almost equal population of j-substates of $n=2$ shell [$\sigma^{\mathrm{exc}}(j=1/2)=1.05$ barns, $\sigma^{\mathrm{exc}}(j=3/2)=0.88$ barns]. Besides, we find that excitation probability into the $2s$ state reaches its maximum at much smaller impact parameters than that for the $2p$ states. This is connected to the relativistic radial contraction of s orbitals occurring for high-Z ions.

In Fig. 3(b) reduced cross sections for simultaneous excitation plus ionization versus impact parameter calculated according to Eq. (1) are shown. Due to its multiplicative nature, the impact parameter dependence of excitation plus ionization exhibits a prominent suppression of probabilities at large impact parameters as compared to the single-electron processes. For example, the probability of simultaneous ionization and excitation into the $2s$ state occurs at a mean impact parameter $b=350$ fm, while the single excitation into this state occurs at a mean impact parameter $b=550$ fm and excitation into the j=3/2 state at $b=1500$ fm. Hence, the cross sections for simultaneous excitation and ionization can be regarded as equivalent to the impact parameter differential measurement in the sense, that they probe the individual single-electron processes for b close to the origin. This in turn is manifested by a strong relative enhancement of excitation plus ionization populating the $2s$ state, i.e., the enhancement of the monopole excitation mode. Indeed, the calculated cross section ratios $\sigma^{\mathrm{exc}}(j=1/2)/\sigma^{\mathrm{exc}}(j=3/2)$ are considerably different for single excitation and excitation accompanied by K-shell ionization, and are equal to 1.19 and 2.36, respectively. This indicates that the measurement of the relative $K\alpha_2$:$K\alpha_1$ and Ly-α_2:Ly-α_1 line ratios, which are easy to resolve experimentally for high-Z ions, can be used as a sensitive tool to study the details of different Coulomb excitation modes.

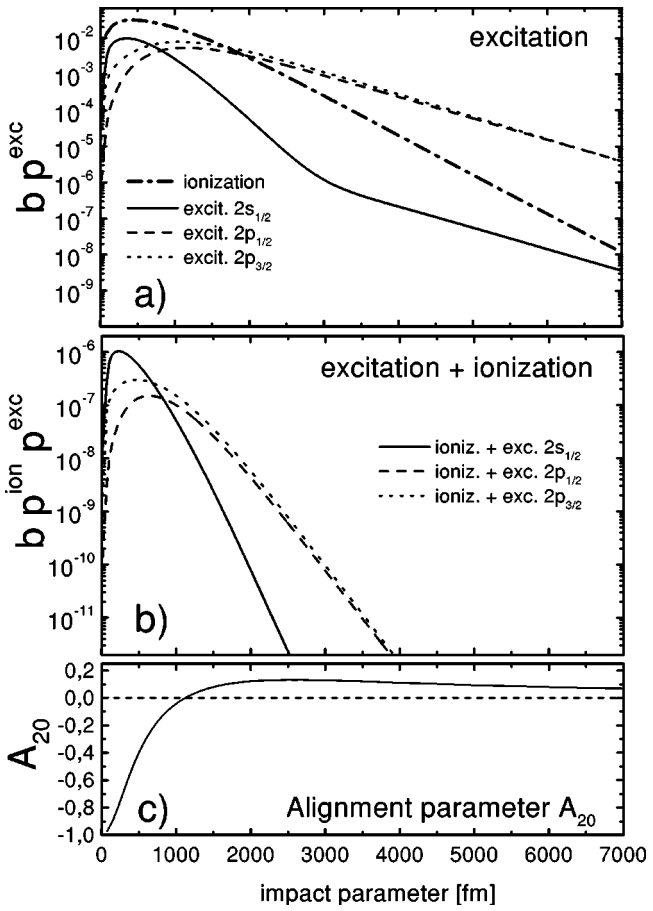

FIG. 3. Calculated probabilities for excitation, excitation-ionization, and the alignment parameter $\mathcal{A}_{20}$ plotted versus collision impact parameter. (a) Reduced probabilities $bp^{\mathrm{exc}}(b)/Z_T^2$ for single excitation of H-like U^{91+} into the $2s_{1/2}$ (—-), $2p_{1/2}$ (— — —), and $2p_{3/2}$ ($\cdots\cdots$), and ionization probability $bp^{\mathrm{ion}}(b)/Z_T^2$($-\,-\,-\cdot-\,-\,-$). (b) Reduced probabilities $bp^{\mathrm{ion}}(b)\times p^{\mathrm{exc}}(b)/Z_T^4$ for simultaneous ionization and excitation into the $2s_{1/2}$ (—-), $2p_{1/2}$ (— — —), and $2p_{3/2}$ ($\cdots\cdots$). (c) Degree of alignment of the $2p_{3/2}$ state.

To investigate further the impact parameter characteristics of excitation and of excitation plus ionization processes, we plot in Fig. 3(c) the degree of alignment of the $2p_{3/2}$ state. The depicted differential alignment parameter $\mathcal{A}_{20}(b)$ defined as

$$\mathcal{A}_{20}(b)=\frac{p^{\rm exc}_{2p3/2|\mu|=3/2}(b)-p^{\rm exc}_{2p3/2|\mu|=1/2}(b)}{p^{\rm exc}_{2p3/2|\mu|=3/2}(b)+p^{\rm exc}_{2p3/2|\mu|=1/2}(b)}, \qquad (5)$$

reflects the relative weights of the population of the magnetic substates (μ) of the $2p_{3/2}$ level by the excitation process. As can be seen in the figure, for small impact parameters the calculated $\mathcal{A}_{20}(b)$ attains large negative values while for more distant collisions the $\mathcal{A}_{20}(b)$ is small and positive. Consequently, for the case of single excitation the integration over impact parameter *b* yields almost no net total alignment ($\mathcal{A}^{\rm exc}_{20}=-0.034$). For simultaneous ionization and excitation, where *b* is confined to small values, the degree of alignment is equal to $\mathcal{A}^{\rm exc\text{-}ion}_{20}=-0.337$ indicating a nonstatistical population of magnetic sub-states of the $2p_{3/2}$ level.

Experimentally, an alignment can be revealed by studying the angular distribution (or polarization) of the de-excitation photons. According to Ref. [34] the angular distribution of x-rays can be expressed with the help of the alignment parameter $\mathcal{A}_{20}$ as:

$$\frac{{\rm d}\sigma}{{\rm d}\Omega}=\frac{\sigma^{\rm tot}}{4\pi}\left\{1+\frac{1}{2}\alpha\mathcal{A}_{20}[3\cos^2(\Theta)-1]\right\} \ {\rm b/sr}, \qquad (6)$$

where α is the anisotropy parameter (equal to 1/2 and 0 for $j=3/2\rightarrow j=1/2$ and $j=1/2\rightarrow j=1/2$ transitions, respectively [34]), Θ is the azimuthal angle of photon emission (in the emitter frame), and $\sigma^{\rm tot}$ is the total cross section for population of the *j*-substate. Hence, the considerably large alignment values predicted for the case of simultaneous ionization and excitation into the $2p_{3/2}$ state, should be reflected in the experiment by an anisotropic angular distribution of the Lyα_1 radiation.

IV. DATA ANALYSIS

A. Normalization of the cross sections

The single and coincidence spectra plotted in Fig. 2 represent the data corrected for a variation of detection efficiency as a function of the photon energy; the coincidence spectra were additionally corrected for random events. Therefore, apart from the normalization factor the line intensities directly reflect the cross sections for the $K\alpha_{1,2}$, $K\beta$, and Ly$\alpha_{1,2}$ production due to the single excitation, and excitation plus ionization processes, respectively.

The most direct and conventionally used way of absolute cross section normalization is based upon the precise knowledge of the target thickness and the beam current. At the specific conditions of the internal gas-jet target at the ESR storage ring, where this experiment was conducted, such factors as the imperfect beam overlap with the gas-jet volume, the limited knowledge of the beam current and uncertainty of the effective gas target density, restrict the accuracy of this method to values not better than approximately 50%. An alternative procedure has been proposed by us recently [36], where these systematic uncertainties are to a large extent eliminated. In this approach, cross sections for arbitrary x-ray production mechanism are determined by normalizing the photon yields to the simultaneously measured number of

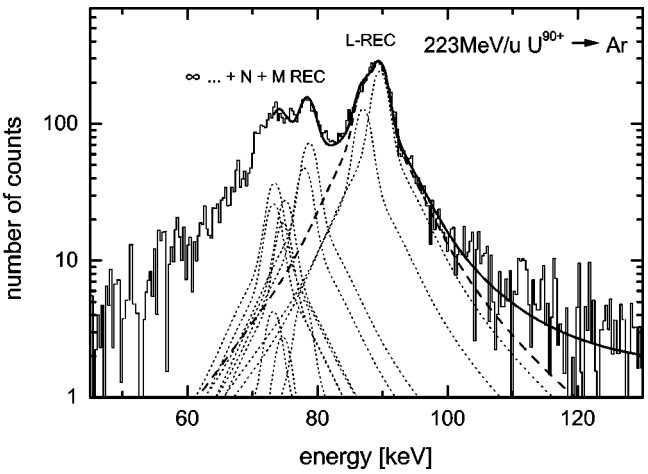

FIG. 4. Radiative electron capture spectrum recorded at 132 ° in coincidence with U^{89+} ions. Data were corrected for x-ray detection efficiency and for random coincidences. Also shown is the result of the least-square fit of the theoretical REC profile. The solid line represents the overall fit result, dotted lines show the contribution of the individual projectile levels, dashed line depicts the contribution of the *L*-REC used for the absolute normalization of simultaneous excitation and ionization cross sections.

REC photons. The cross sections for the REC process, can be obtained from the new generation of fully relativistic calculations with a high accuracy (see, e.g., Refs. [17,18] and [37]). Following Ref. [36], we adopt this method also here, making use of the fact that the cooled ion beams and gas targets used, guarantee that REC is observed in the exceptionally clean experimental conditions.

The number of REC photons was determined from a least-square fit of the theoretical line profile to the experimental data. Figure 4 shows a sample REC spectrum registered for uranium on an argon target in coincidence with a particle detector counting U^{89+} ions. Since in our case, the *K* shell of the projectile is occupied, only REC leading to the *L*, *M*, and higher projectile shells, can be observed. Therefore, for the absolute cross-section normalization the most abundant REC into the *L* shell was chosen. The line profiles used in the fit were constructed exploiting the tabulated Compton profiles for target atoms [38], and using the binding energies for Li-like uranium calculated with the multi-configuration Dirac-Fock code GRASP [39]. Since, due to the large width of Compton profile for Ar, Kr, and Xe targets, the *L*-REC partially overlaps with the tails of REC into *M*-, and higher levels, the latter capture modes were also considered in the fits. The different total angular momentum states of the projectile with principal quantum number up to $n=5$ were taken into account (see dotted lines in Fig. 4). The dashed line in Fig. 4 shows the fitted *L*-REC line profile used for normalization purposes.

For all targets considered, the absolute normalization of cross sections was based on the *L*-REC intensity observed at 132 °. The normalization of photon yields observed at 48 ° and 90 ° was based on the precisely known geometry of the detector setup. The overall uncertainty of the normalization procedure is smaller than 10% in the case of the Ar target.

For the Xe target, overall uncertainty reaches 20% due to counting statistics and the uncertainty of the model.

B. Cascade corrections

While the ground-state Coulomb excitation leads preferably to the population of $n=2$ states [23], a small fraction of electrons can be promoted to states with principal quantum number $n>2$. The de-excitation of the latter may in turn feed the $n=2$ states. Therefore, to compare the experimental data with theory, the observed line intensities have to be corrected for this effect. For this purpose, the cascade decay of excited states was modeled using theoretical cross sections for excitation into the individual projectile substates with $n\leqslant 4$, and adopting the decay branching ratios obtained from MCDF code GRASP [39]. This model has been proved to be succesful in predicting the single excitation of H-like systems (see, e.g., [23] and [24]), where excellent agreement is found between calculations and the x-ray spectra, in which transitions up to the *K*-series limit are observed. In case of the excitation-ionization, calculations showed that the cascade decay into the $n=2$ states contribute about 24% and 5% to the Lyα_1 and Lyα_2 production cross sections, respectively.

V. RESULTS AND DISCUSSION

A. Angle differential cross sections

In Fig. 5, a comparison of experimental and theoretical cross sections for simultaneous ionization and excitation into the $n=2$ states of He-like uranium ions is presented as a function of observation angle.

To show the angular characteristics of the emitted radiation in the absence of Lorentz transformation effects, the differential cross sections are corrected for the relativistic solid angle transformation. The error bars shown in the figure represent both the statistical uncertainties of the measured Lyα_1 and Lyα_2 lines, as well as uncertainty of the normalization procedure applied to determine the absolute cross section values.

The theoretical differential cross sections for ionization and excitation into the $n=2$ levels with total angular momentum $j=1/2$ and $j=3/2$ are represented in Fig. 5 by solid and dashed lines, respectively. The curves were calculated according to Eq. (6) adopting the theoretical values of excitation cross sections into the individual j substates of $n=2$ shell and using the calculated alignment parameter $\mathcal{A}_{20}$. For the Ar target the measured and calculated differential cross sections for simultaneous excitation and ionization are in good agreement. In particular, the predicted angular characteristics of the emitted radiation, and the dominance of the excitation into the $j=1/2$ states, is well reproduced experimentally. For heavier targets the experimental data are generally smaller than calculated.

B. Total excitation-ionization cross sections

Figure 6 shows the total cross sections for simultaneous ionization and excitation of the two ground state electrons of He-like uranium plotted versus target atomic number. The

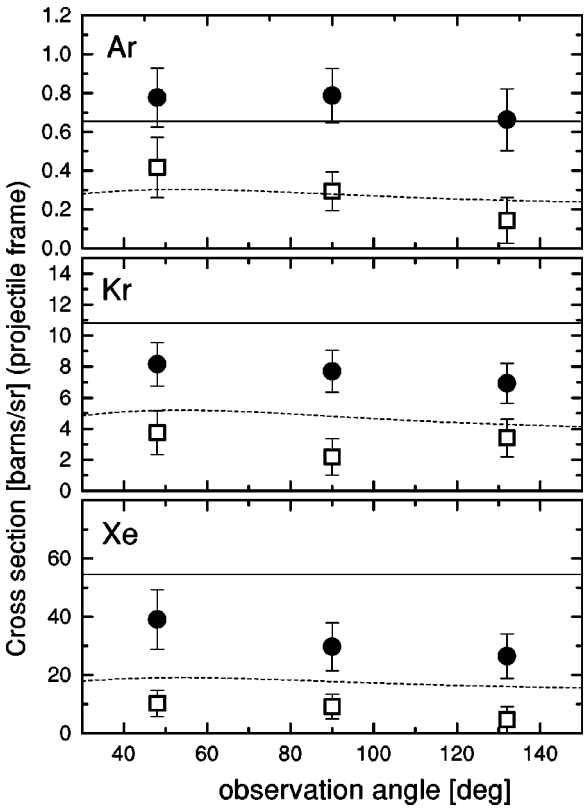

FIG. 5. Angle differential cross sections (projectile frame) for simultaneous ionization and excitation of 223.2 MeV/u U^{90+} ions in collisions with Ar, Kr, and Xe gas targets. The solid circles and open squares represent experimental data for simultaneous ionization and excitation into the projectile *L*-shell states with total angular momentum $j=1/2$ and $j=3/2$, respectively. The theoretical predictions are given by solid ($j=1/2$) and dashed ($j=3/2$) lines.

experimental values were obtained from a least-squares fit of Eq. (6) to the angle differential data, assuming one adjustable parameter σ^{tot}. The results are compared to the relativistic IPA calculations (see Sec. III) of the simultaneous ionization and excitation into the individual *j*-sub-states of the projectile *L* shell.

From the comparison given in Figs. 5 and 6 a good overall agreement can be stated for the Ar target. It should be noted, that for the description of individual single electron processes a theoretical approach based on the relativistic formalism was used. More specifically, the ionization process was treated in a semirelativistic way, i.e., the correct electronic wave functions were used, but the magnetic part of the interaction potential was neglected. This approach seems to be rather well justified, since the existing experimental data show that the *K*-shell ionization is rather insensitive to the relativistic corrections [13,12], for $\beta\ll 1$. Unlike for ionization, the fully relativistic approach has been found to be essential for the case of projectile excitation [23,24]. In particular, it has been demonstrated for the ground state excitation of H-and He-like Bi ions, that the inclusion of the magnetic interaction leads to a strong increase of the relative amplitude of the transitions with $\mu_f=\mu_i-1$, over the entire range of impact parameters [23]. Good agreement between

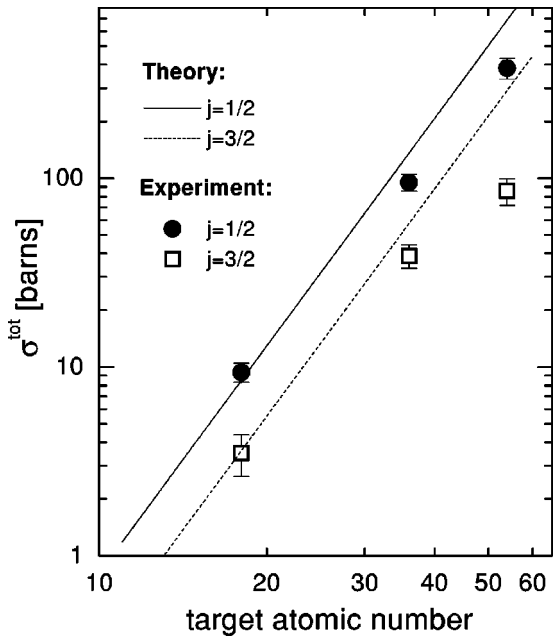

FIG. 6. The total cross sections for simultaneous ionization and excitation of U^{90+} ions in collisions with Ar, Kr, and Xe gas targets at an incident energy of 223.2 MeV/u. The experimental data are given separately for excitation into the $j=1/2$ (full circles) and $j=3/2$ (squares) L-shell states of the U^{91+}. The solid and dashed lines depict the theoretical predictions.

the experimental data and the calculations for the Ar target, supports the conclusion of the earlier work.

It is worthwhile to recall here the difference of the impact parameter dependence between the single-electron processes and simultaneous excitation and ionization discussed in Sec. III C. In the first case, an effective range of impact parameters is determined by the size of the electron orbital, in the second case, only small impact parameters contribute significantly to the total cross sections. For such near central collisions, the perturbation generated by the target nucleus is largest. Hence, the measurement of two-electron processes tests more stringently the applicability of the perturbation theory than does the measurement of single electron cross-sections. Our results for heavy (Kr and Xe) targets show that the process of simultaneous excitation and ionization cannot be described perturbatively to within the accuracy of better than 50%.

To investigate further the features of the excitation-ionization process, in Fig. 7 we plot the cross-section ratios $\sigma^{\text{exc-ion}}(j=1/2)/\sigma^{\text{exc-ion}}(j=3/2)$ (triangles) versus target nuclear charge. This presentation of the data allows us to eliminate systematic errors due to the uncertainty of the absolute cross section normalization.

As pointed out in Sec. III C the population patterns of the projectile $j-$sub-states markedly differ for single excitation and simultaneous ionization and excitation. For the excitation-ionization process the monople $(1s\rightarrow 2s)$ excitation mode is strongly favored with respect to the dipole one $(1s\rightarrow 2p)$, as compared to the single excitation (see dashed line in Fig. 7). This is a consequence of the impact parameter characteristics of these two processes. The predicted relative

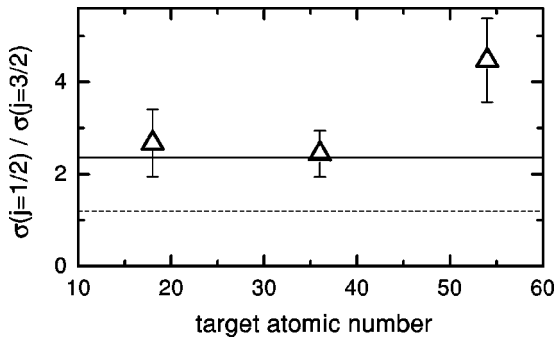

FIG. 7. The theoretical (solid line) and experimental (△) cross section ratios for the population of $j=1/2$ and $j=3/2$ by the excitation-ionization process. For illustration, the predicted cross section ratios for single excitation $\sigma^{\text{exc}}(j=1/2)/\sigma^{\text{exc}}(j=3/2)$ are given (dashed line).

enhancement of ionization and excitation into $j=1/2$ states is well reproduced experimentally, for the case of the Ar and Kr targets. For the Xe target the ratio $\sigma^{\text{exc-ion}}(j=1/2)/\sigma^{\text{exc-ion}}(j=3/2)$ is considerably larger than calculated. This is likely connected to the failure of the first-order perturbation theory for this energy-target atomic number regime. Additional evidence for the breakdown of first order perturbation theory for heavy targets can be found in Fig. 2. In the plot, a variation of the relative intensity of Lyα_1 and Lyα_2 lines with the target nuclear charge can be observed. It is interesting to note that this effect is present in the case of single excitation (Fig. 2, upper plot) as well.

C. Electron-electron interaction

When dealing with many-electron processes, generally an interaction between them has to be taken into account. In the process of simultaneous excitation and ionization, where final electron states differ, an overall transition amplitude can potentially be sensitive to the ground state electron-electron interaction. In this context, helium-like uranium is a particularly interesting system, since here the ground state electron-electron interaction is the largest among all stable elements, while simultaneously both electrons experience the strongest Coulombic field of the nucleus. Therefore, as an archetypal two-electron high-Z ion, it offers the simplest possible testing ground for the studies of electron-electron interaction effects in ion-atom collisions.

The multi-electron processes in relativistic ion-atom collisions have been investigated up to date only for the case of multiple electron ionization and multiple capture [40]. In that case the IPA has been shown to be rather successful in predicting the total cross sections. The good agreement found in the present work for the Ar target, where the validity of first order perturbation theory is unquestionable, also gives no indication of the existence of correlation in simultaneous ionization and excitation of the He-like uranium system. However, to critically judge whether correlation effects are of importance for excitation-ionization process, statistically more significant experimental data are needed.

VI. SUMMARY

In this paper we report on the investigation of the two-electron (excitation plus ionization) process occurring in relativistic collisions of very heavy highly charged ions with gaseous matter. The measurements were performed for He-like uranium allowing us to study of two-electron processes in the absence of spectator electrons. In the experiment Lyman-series radiation of 223.2 MeV/u initially He-like uranium ions impinging upon gaseous targets has been measured at various observation angles in coincidence with projectiles that gained one charge state. The gas-targets used, ensured that the probability of excitation and ionization in two consecutive collisions is negligible. Hence, the simultaneous excitation plus ionization could be unambiguously identified by the requirement of coincident observation of the projectile Lyα emission and projectile ionization. The x-ray yields were used to deduce the cross sections for simultaneous ionization and excitation into the $j=1/2$ and $j=3/2$ levels of the projectile L shell. Measurements have been performed for Ar, Kr, and Xe targets providing the information about the population yields of the excited states as a function of the strength of the perturbing potential.

The applied experimental technique along with the novel method of the absolute cross section normalization, provided the first and reliable data for the excitation-ionization processes in the domain of relativistic collisions and high-Z two-electron systems. In the discussion, we underline the sensitivity of the measured cross sections to the properties of the excitation probabilities at small impact parameters. Such impact parameter selective data are difficult to access experimentally by the direct measurement.

The angle-differential and total cross sections for simultaneous excitation and ionization have been compared with relativistic calculations of the excitation and ionization derived on the basis of the independent particle approximation and first order perturbation theory. Our experimental data has provided a good test of the validity of these models and supported these approximations for Ar target. The data for the Kr and Xe targets point to the inadequacy of first order perturbation theory for the description of simultaneous excitation and ionization.

ACKNOWLEDGMENTS

We would like to thank Professor J. Eichler and A. Ichihara for providing us with the theoretical REC cross sessions. The SCA program code was provided by Professor D. Trautmann. The work of two of us (Z.S. and A.W.) was supported in part by the State Committee for Scientific Research KBN (Poland) under Research Grant No. 2P03B10910 and by GSI-Darmstadt. R.W.D. was supported by GSI and the U.S. DOE Office of Basic Energy Sciences, Division of Chemical Science. P.R. was supported by GSI and by the State Committee for Scientific Research KBN (Poland) under Research Grant No. 2P03B 116 15.

[1] R. Anholt and H. Gould, in *Advances in Atomic and Molecular Physics* Vol. 22, edited by D. Bates and B. Bederson (Academic Press, Orlando, 1986) p. 315.

[2] J. Eichler and W. E. Meyerhof, *Relativistic Atomic Collisions* (Academic Press, San Diego, 1995).

[3] R. Anholt, Ch. Stoller, J. D. Molitoris, D. W. Spooner, E. Morenzoni, S. A. Andriemonje, W. Meyerhof, H. Bownamm, J.-S. Xu, Z.-Z. Xu, J. O. Rasmussen, and D. H. H. Hoffmann, Phys. Rev. A **33**, 2270 (1986).

[4] W. E. Meyerhof, R. Anholt, J. Eichler, H. Gould, Ch. Munger, J. Alonso, P. Thieberger, and H. E. Wegner, Phys. Rev. A **32**, 3291 (1985).

[5] Th. Stöhlker, H. Geissel, H. Irnich, T. Kandler, C. Kozhuharov, P. H. Mokler, G. Münzenberg, F. Nickel, C. Scheidenberger, T. Suzuki, M. Kucharski, A. Warczak, P. Rymuza, Z. Stachura, A. Kriessbach, D. Dauvergne, R. Dunford, J. Eichler, A. Ichiharaz, and T. Shirai, Phys. Rev. Lett. **73**, 3520 (1994).

[6] Th. Stöhlker, C. Kozhuharov, P. H. Mokler, A. Warczak, F. Bosch, H. Geissel, R. Moshammer, C. Scheidenberger, J. Eichler, A. Ichihara, T. Shiraio, Z. Stachura, and P. Rymuza, Phys. Rev. A **51**, 2098 (1995).

[7] A. Belkacem, N. Claytor, T. Dinneen, B. Feinberg, and H. Gould, Phys. Rev. A **58**, 1253 (1998).

[8] A. Belkacem, H. Gould, B. Feinberg, R. Bossingham, and W. E. Meyerhof, Phys. Rev. A **56**, 2806 (1997).

[9] H. F. Krause, C. R. Vane, S. Datz, P. Grafström, H. Knudsen, C. Scheidenberger, and R. H. Schuch, Phys. Rev. Lett. **80**, 1190 (1998).

[10] R. Anholt, W. E. Meyerhof, Ch. Stoller, E. Morenzoni, S. A. Andriamonje, J. D. Molitoris, O. K. Baker, D. H. H. Hoffmann, H. Bowman, J.-S. Xu, Z.-Z. Xu, K. Frankel, D. Murphy, K. Crowe, and J. O. Rasmussen, Phys. Rev. A **30**, 2234 (1984).

[11] A. Westphal and Y. D. He, Phys. Rev. Lett. **71**, 1160 (1993).

[12] R. Anholt, W. E. Meyerhof, H. Gould, Ch. Munger, J. Alonso, P. Thieberger, and H. E. Wegner, Phys. Rev. A **32**, 3302 (1985).

[13] Th. Stöhlker, D. C. Ionescu, P. Rymuza, T. Ludziejewski, P. H. Mokler, C. Scheidenberger, F. Bosch, B. Franzke, H. Geissel, O. Klepper, C. Kozhuharov, R. Moshammer, F. Nickel, H. Reich, Z. Stachura, and A. Warczak, Nucl. Instrum. Methods Phys. Res. B **124**, 160 (1997).

[14] N. Claytor, A. Belkacem, T. Dinneen, B. Feinberg, and H. Gould, Phys. Rev. A **55**, R842 (1997).

[15] G. Mehler, G. Soff, K. Rumrich, and W. Greiner, Z. Phys. D: At., Mol. Clusters **13**, 193 (1989).

[16] U. Becker, N. Grün, W. Scheid, and G. Soff, Phys. Rev. Lett. **56**, 2016 (1986).

[17] A. Ichihara, T. Shirai, and J. Eichler, Phys. Rev. A **49**, 1875 (1994).

[18] J. Eichler, A. Ichihara, and T. Shirai, Phys. Rev. A **51**, 3027 (1995).

[19] C. Ionescu (private communication) (see also Refs. [23] and [24]).

[20] K. Momberger, N. Grün, W. Scheid, and U. Becker, J. Phys. B **23**, 2293S (1990).
[21] K. Momberger, A. Belkacem, and A. H. Sørensen, Phys. Rev. A **53**, 1605 (1996).
[22] C. Bottcher and M. R. Strayer, Phys. Rev. Lett. **54**, 996 (1985).
[23] Th. Stöhlker, D. C. Ionescu, P. Rymuza, F. Bosch, H. Geissel, C. Kozhuharov, T. Ludziejewski, P. H. Mokler, C. Scheidenberger, Z. Stachura, A. Warczak, and R. W. Dunford, Phys. Rev. A **57**, 845 (1998).
[24] Th. Stöhlker, D. C. Ionescu, P. Rymuza, F. Bosch, H. Geissel, C. Kozhuharov, T. Ludziejewski, P. H. Mokler, C. Scheidenberger, Z. Stachura, A. Warczak, and R. W. Dunford, Phys. Lett. A **238**, 43 (1998).
[25] J. H. McGuire, Adv. At., Mol., Opt. Phys. **29**, 217 (1992).
[26] J. O. P. Pedersen and F. Folkmann, J. Phys. B **23**, 441 (1990).
[27] D. Vernhet, L. Adoui, J. P. Rozet, K. Wohrer, A. Chetioui, A. Cassimi, J. P. Grandin, J. M. Ramillon, M. Cornille, and C. Stephan, Phys. Rev. Lett. **79**, 3625 (1977).
[28] P. A. Hayes and J. F. Williams, Phys. Rev. Lett. **77**, 3098 (1996).
[29] J. Bang, J. M. Hansteen, and Kgl. Danske Videnskab Selskab, Mat. Fys. Medd. K. Dan. Vidensk. Selsk. **31**, 13 (1959).
[30] D. Trautmann and F. Rösel, Nucl. Instrum. Methods **169**, 259 (1980).
[31] W. R. Johnson and G. Soff, At. Data Nucl. Data Tables **33**, 405 (1985).
[32] R. Anholt, Phys. Rev. A **19**, 1004 (1979).
[33] R. Anholt and U. Becker, Phys. Rev. A **36**, 4628 (1987).
[34] E. G. Berezhko and N. M. Kabachnik, J. Phys. B **10**, 2427 (1977).
[35] A. Derevianko and W. R. Johnson, Phys. Rev. A **56**, 1288 (1997).
[36] Th. Stöhlker, T. Ludziejewski, H. Reich, F. Bosch, R. W. Dunford, J. Eichler, B. Franzke, C. Kozhuharov, O. Klepper, G. Menzel, P. Mokler, F. Nolden, P. Rymuza, Z. Stachura, M. Steck, P. Świat, and A. Warczak, Phys. Rev. A **58**, 2043 (1998).
[37] A. Ichihara, T. Shirai, and J. Eichler, Phys. Rev. A **54**, 4956 (1996).
[38] F. Biggs, L. B. Mendelsohn, and J. Mann, At. Data Nucl. Data Tables **16**, 201 (1975).
[39] K. G. Dyall, I. P. Grant, C. T. Johnson, F. A. Parpia, and E. P. Plummer, Comput. Phys. Commun. **55**, 425 (1989).
[40] W. E. Meyerhof, R. Anholt, X-Y. Xu, H. Gould, B. Feinberg, R. J. McDonald, H. E. Wegner, and P. Thieberger, Nucl. Instrum. Methods Phys. Res. A **262**, 10 (1987).